CRYSTAL GROWTH & DESIGN

pubs.acs.org/crystal

Article

Organic Controls over Biomineral Ca−Mg Carbonate Compositions and Morphologies

Yihang Fang,* Seungyeol Lee, Huifang Xu, and Gabriela A. Farfan*

Cite This: *Cryst. Growth Des.* 2023, 23, 4872−4882

Read Online

ACCESS | Metrics & More | Article Recommendations | Supporting Information

ABSTRACT: Calcium carbonate minerals, such as aragonite and calcite, are widespread in biomineral skeletons, shells, exoskeletons, and more. With rapidly increasing pCO_2 levels linked to anthropogenic climate change, carbonate minerals face the threat of dissolution, especially in an acidifying ocean. Given the right conditions, Ca−Mg carbonates (especially disordered dolomite and dolomite) are alternative minerals for organisms to utilize, with the added benefit of being harder and more resistant to dissolution. Ca−Mg carbonate also holds greater potential for carbon sequestration due to both Ca and Mg cations being available to bond with the carbonate group (CO_3^{2-}). However, Mg-bearing carbonates are relatively rare biominerals because the high kinetic energy barrier for the dehydration of the Mg^{2+}−water complex severely restricts Mg incorporation in carbonates at Earth surface conditions. This work presents the first overview of the effects of the physiochemical properties of amino acids and chitins on the mineralogy, composition, and morphology of Ca−Mg carbonates in solutions and on solid surfaces. We discovered that acidic, negatively charged, hydrophilic amino acids (aspartic and glutamic) and chitins could induce the precipitation of high-magnesium calcite (HMC) and disordered dolomite in solution and on solid surfaces with these adsorbed biosubstrates via *in vitro* experiments. Thus, we expect that acidic amino acids and chitins are among the controlling factors in biomineralization used in different combinations to control the mineral phases, compositions, and morphologies of Ca−Mg carbonate biomineral crystals.

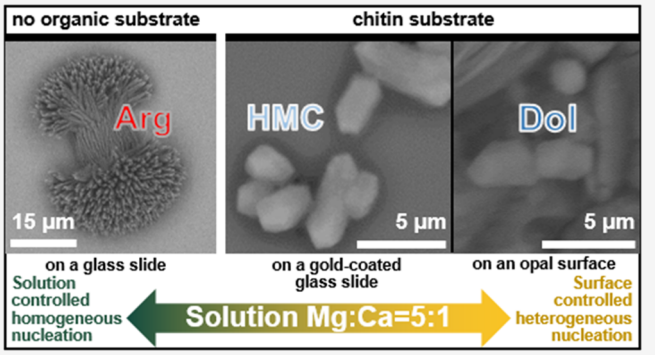

INTRODUCTION

Calcium carbonate minerals are the most common mineral components in biominerals across geologic time, ranging from the Neoproterozoic to the present.[1] From algae,[2] foraminifera,[3] coral,[4] mollusks,[5] and echinoderms[6] in aquatic environments, to ants,[7] gastropods,[8] and humans[9] on land, biocarbonates are observed across a wide range of environments and organisms across the tree of life. Apart from serving as biomineral shells and skeletons, carbonates also play an important role in the global carbon cycle by sequestering carbon in long-term mineral storage and regulating the carbonate chemistry and pH of the ocean.[10] Finally, they preserve vital records of biological and geological evolution on Earth as fossils.[11]

Compared to pure calcium carbonate species such as calcite and aragonite, Mg-bearing calcium carbonates such as high-magnesium calcite (HMC), proto-dolomite, and disordered dolomite (Dol) are known to be more resistant to physical weathering and are potentially more imperviable to dissolution in an acidifying ocean.[12] Mg-bearing calcium carbonate could potentially serve as a better carbon sink by utilizing Mg^{2+} cations, which are abundant in natural water. However, the occurrence of Mg-bearing carbonates in modern-day systems is incredibly rare compared to pure calcium carbonate phases and has only been occasionally reported in organisms such as corals,[13] mollusks,[14,15] sea urchins,[16] and ants.[7] This limited occurrence stems from the reluctance of magnesium cations to dehydrate in low-temperature environments, inhibiting magnesium from being incorporated into carbonates with calcite structures.[17,18]

Synthetic experiments testing the mechanisms of high-Mg calcium carbonate formation demonstrated that homogeneous nucleation in the presence of dissolved silica,[19] sulfide,[20] polysaccharides,[21] exopolymeric substances (EPS),[22,23] and amphipathic molecules such as ethanol (and likely others with similar polarity/acidic/hydrophilicity properties) dehydrates the local mineral surface to allow for Mg incorporation into Ca−Mg carbonate.[17] Here, we examine how biomolecules commonly observed in biominerals, such as amino acids and chitins, may be involved in Mg incorporation in Ca−Mg carbonates. Previous works have demonstrated how various

Received: January 31, 2023
Revised: April 27, 2023
Published: May 31, 2023

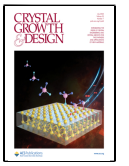

https://doi.org/10.1021/acs.cgd.3c00102
Cryst. Growth Des. 2023, 23, 4872−4882

Table 1. Amino Acid and Chitin Physicochemical Properties and the Resulting Carbonate Phases Precipitated in Solution with Starting Concentrations of $[Mg^{2+}]$ = 31.25 mM, $[Ca^{2+}]$ = 6.25 mM, $[CO_3^{2-}]$ = 50 mM, and 20 mM of Organic Substrate (0.1 g/L for Chitin)[a]

substrate	polarity	charge at pH = 7.4	hydropathy index	hydrophobic/hydrophilic	physiochemistry class	precipitation in solution	$MgCO_3$ mol %
aspartic acid	polar	negative	−3.5	hydrophilic	acidic	aragonite + HMC	21.80
glutamic acid	polar	negative	−3.5	hydrophilic	acidic	aragonite + HMC	21.60
glycine	nonpolar	neutral	−0.4	hydrophilic	aliphatic	aragonite	
isoleucine	nonpolar	neutral	3.8	hydrophobic	aliphatic	aragonite	
leucine	nonpolar	neutral	4.5	hydrophobic	aliphatic	aragonite	
lysine	polar	positive	−3.9	hydrophilic	basic	aragonite	
phenylalanine	nonpolar	neutral	2.8	hydrophobic	aromatic	aragonite	
serine	polar	neutral	−0.8	hydrophilic	hydroxylic	aragonite	
chitin						aragonite + HMC	21.85

[a]Detailed structures of amino acids and chitin can be found in Table S2.

Table 2. Experimental Conditions for Solid Surface Experiments and Their Resulting Mineral Phases and mol % $MgCO_3$ in Calcite-Structure Carbonate[a]

substrate	surface	substrate concentration	$[Mg^{2+}]$ (mM)	$[Ca^{2+}]$ (mM)	precipitation phases	d_{104} (Å)	$MgCO_3$ mol %
aspartic acid	solution	7.5 mM	31.25	6.25	aragonite + HMC	2.976	21.8
	Opal				aragonite + HMC	2.958	27.4
	GCGS				aragonite + Mg-cal	2.999	12.9
	GS				aragonite + Mg-cal	3.008	9.9
chitin	solution	0.0375 g	31.25	6.25	aragonite + HMC	2.974	21.9
	Opal				aragonite + Dol	2.931	46.3
	GCGS				aragonite + HMC	2.949	35.1
	GS				aragonite + HMC	2.953	32.3
control	solution		31.25	6.25	aragonite + calcite[b]		
	Opal				aragonite + calcite[b]		
	GCGS				aragonite + calcite[b]		
	GS				aragonite + calcite[b]		

[a]$MgCO_3$ values were calculated based on d_{104} values of the calcite -structure carbonates following procedures from Fang and Xu.[32] [b]Denotes a trace amount.

amino acids and chitin have direct effects on $CaCO_3$ precipitation in mollusks,[5] chitons,[7,24] foraminifera,[25] and corals.[26] Some biomineral species even display different amino acid compositions in aragonite versus calcite regions of coral skeletons[4] and mollusks shells.[27−29] Yet, the effect of these different biosubstrates on Mg incorporation in calcium carbonates and their resulting morphologies has not been previously tested.

In this study, we explore how different amino acids and chitin may be involved in Mg carbonate precipitation in biomineralization systems. We used mineralogical and geochemical approaches to precipitate synthetic Ca−Mg carbonates via *in vitro* experiments in solutions with various solid substrate surfaces to examine the final Mg concentrations and morphologies of the precipitates.

METHODS

Synthesis Experiments. *In vitro* synthesis experiments were conducted in polyethylene bottles at room temperature (20 °C). Eight different amino acids were tested to probe the effect of different amino acid properties, such as polarity, hydrophilicity, and acidity, on carbonate formation (Table 1). Amino acids (7.5 mM) and chitin (0.025 g/L) were mixed into 50 mL of deionized (DI) water and continuously stirred in polyethylene bottles for half an hour. Then, 6.25 mM calcium chloride dihydrate ($CaCl_2{\cdot}2H_2O$), 31.25 mM magnesium chloride hexahydrate ($MgCl_2{\cdot}6H_2O$), and 25 mM sodium bicarbonate ($NaHCO_3$) were dissolved into the organic substrate bearing solutions. After another 30 min of mixing, to ensure that everything had dissolved, the bottles were sealed and kept at room temperature. After a week, solutions were filtered and air-dried.

In a separate set of experiments to test the effects of solid surfaces on Ca−Mg carbonate precipitation, aspartic acid, glutamic acid, and chitin were first individually mixed with deionized (DI) water. Natural amorphous opal-A (opal) slices from Australia, glass slides (GS), and gold-coated glass slides (GCGS) were then placed into these solutions for 24 h with closed lids to allow solutes to adsorb onto their surfaces. Next, calcium chloride dihydrate ($CaCl_2{\cdot}2H_2O$) and magnesium chloride hexahydrate ($MgCl_2{\cdot}6H_2O$) were added to the solutions to provide the Ca and Mg needed to precipitate Ca−Mg carbonate minerals (see Table 2 for solution concentrations). In most solutions, the initial Mg/Ca ratio was set to 5 as an analogue to the seawater Mg/Ca ratio (∼5); however, some solutions had lower Mg/Ca ratios of 3−2 (Table S1). Absolute concentrations of Mg range from 40 to 20 mM (Table S1). Polyethylene bottles containing these solutions (100 mL each) were placed into a sealed desiccator with ammonium bicarbonate ($[NH_4]HCO_3$) powders (20 g), allowing for NH_3 and the necessary CO_2 to diffuse into the open-lid solutions for the carbonate minerals to precipitate. After one week, the solutions were removed from the desiccators, and precipitates were filtered out with 20−25 μm pore-size filter papers. Surface materials, i.e., opal, GS, and GCGS, were picked out and rinsed with DI water for 30 seconds to remove precipitates that had been formed in the solution but settled on the surfaces, leaving behind only the minerals that precipitated directly onto the solid surfaces.

Analytic Procedures. X-ray diffraction (XRD) analyses were conducted using a Rigaku Rapid II XRD system (Mo Kα radiation, λ = 0.7093 Å) equipped with a two-dimensional (2D) image-plate detector in the S.W. Bailey X-ray Diffraction Laboratory in the Department of Geoscience at the University of Wisconsin-Madison.

https://doi.org/10.1021/acs.cgd.3c00102
Cryst. Growth Des. 2023, 23, 4872−4882

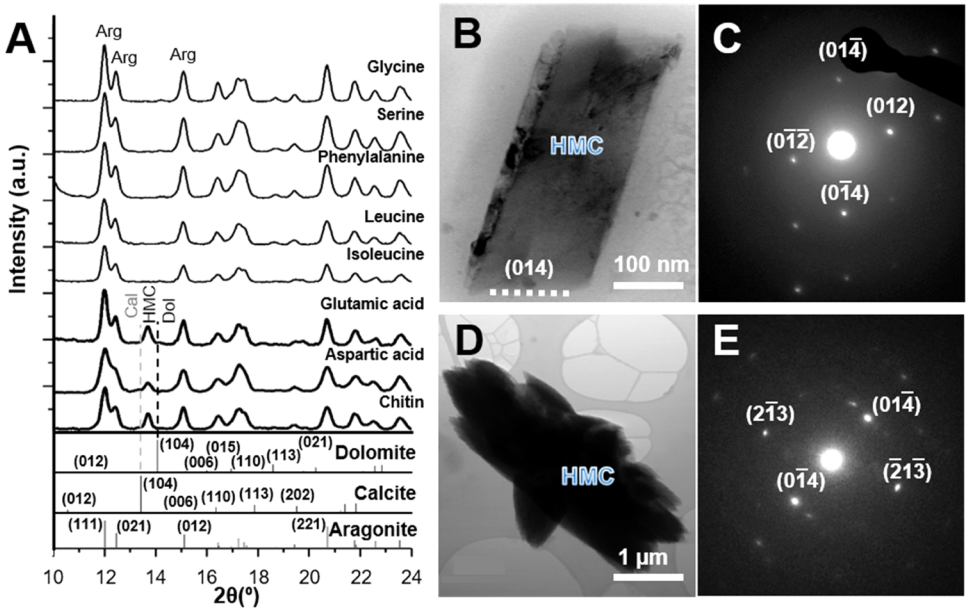

Figure 1. Mineralogical analyses of precipitates from biosubstrate-rich solutions. (A) X-ray powder diffraction patterns (Mo Kα) of precipitates formed with different amino acids and chitin solutions. Patterns in bold lines show the presence of high-Mg calcite (HMC) phases with (104) peak positions located between the calcite and dolomite standards. (B) Transmission electron microscopy (TEM) image of HMC formed on a chitin-coated opal surface. (C) Selected-area electron diffraction (SAED) patterns of (B) along [100] zone axis showing distinct "*a*"-reflections indicating large coherent domains and no "*b*"-reflection suggesting no Ca−Mg cation ordering. (D) TEM image of HMC formed in an aspartic acid solution. (E) SAED pattern of (D) along the [182] zone axis showing distinct *a*-reflections indicating large coherent domains and no *b*-reflection suggesting no Ca−Mg cation ordering.

Diffraction patterns were collected on the image-plate detector and integrated using Rigaku 2DP software. Mineral phases were identified using the MDI Jade 9.5 software package with the American Mineralogist Crystal Database (AMCSD) and the PDF-4+ database from the International Centre for Diffraction Data (ICDD). Rietveld refinements calculated unit cell parameters, crystal sizes, phase fractions, and crystallinity using the Bruker TOPAS program and crystal structures from the AMCSD. Pearson VII peak functions were used for all refinements. We used the d_{104} values of calcite and dolomite structures to estimate $MgCO_3$ percentages in Ca−Mg carbonates based on an empirical curve from previous works.[30,31]

Scanning electron microscopy (SEM), X-ray energy-dispersive spectroscopy (EDS), and electron backscatter diffraction (EBSD) were conducted using a Hitachi S3400 equipped with Oxford Aztec EDS and EBSD systems at the Department of Geoscience at the University of Wisconsin-Madison. EDS imaging, including backscatter electron (BSE) imaging and secondary electron (SE) imaging, and EDS, was conducted at 15 kV with a horizontal setting. EBSD was performed at 20 kV with a 70° tilt. All samples were coated with 1 nm thick iridium to prevent charging. The EDS results were calibrated with a dolomite standard (Delight dolomite) with the published value of 50.48 mol % $MgCO_3$.[2121] Additional SEM images were collected using a Thermofisher Quattro S ESEM at the Institute of Materials Science & Engineering at the Washington University in St. Louis.

The samples were analyzed using a JEOL 7600F field-emission-gun scanning transmission electron microscope at NASA Johnson Space Center (JSC) to obtain high-resolution transmission electron microscopy (HRTEM) images. Chemical compositions were characterized using a JEOL SD60GV 60 mm^2 ultrathin window silicon drift detector (SDD). A combination of spot analyses and element maps was collected from each sample to understand element distributions, abundances, and ratios. The energy-dispersive X-ray (EDX) mapping analyses were obtained using a 2 nm probe to reduce beam damage and showed the spatial distribution of major and minor elements.

Raman spectra were collected on a subset of experiment samples using a Horiba LabRAM Evolution Raman system with a CCD detector at the Smithsonian National Museum of Natural History in the Department of Mineral Sciences. We used an unpolarized 532 nm green laser coupled with an 1800 groove grating to collect spectra from 50 to 4000 cm^{-1} Raman shift. Each spectrum was an average of five replicates collected for five seconds each at a 10% laser power (using neutral density filters) of approximately 4.4 mW. The spot size of the laser using the 100× objective was <5 μm in diameter. The laser was calibrated using a Si wafer and laser power measurements were made with a ThorLabs S170C Microscope Slide Power Sensor system on a silicon wafer. Representative Raman spectra of dolomite (NMNH161804, Penfield Quarry, Rochester, NY), low-Mg calcite (NMNH144953-33, Iceberg claim, Copper Mountain Mining District, Taos Co., NM), and aragonite (NMNHB10095, Spania Dolina, Slovakia) were collected from mineral samples from the Smithsonian National Gem and Mineral Collection, and are referred to as "standards."

RESULTS

Mineralogy of Synthetic Ca−Mg Carbonate Precipitates in Solution with Organic Substrates. XRD results show that suspended precipitates formed in solution with aspartic acid (Asp) and glutamic acid (Glu) are dominated by high-magnesium calcite (HMC; d_{104} = 2.9755 and 2.9756 Å corresponding to 21.8 and 21.6 mol % $MgCO_3$ for aspartic acid and glutamic acid) with aragonite (Figure 1 and Table 1). Other amino acids (glycine, isoleucine, leucine, lysine, phenylalanine, serine) resulted in aragonite precipitation in the solution (Figure 1 and Table 1). Similar to the aspartic acid and glutamic acid experiments, chitin experiments also resulted in precipitates composed of HMC (d_{104} = 2.9754 Å corresponding to 21.9 mol % $MgCO_3$; Figure 1 and Table 1).

TEM results confirm the presence of HMC in aspartic acid and chitin experiments and show that HMC crystals from synthesis experiments lack cation ordering with the absence of *b*-reflections typically observed in natural dolomite (Figure 1B−E; 30). *b*-Reflections originate from the reduced symmetry

https://doi.org/10.1021/acs.cgd.3c00102
Cryst. Growth Des. 2023, 23, 4872−4882

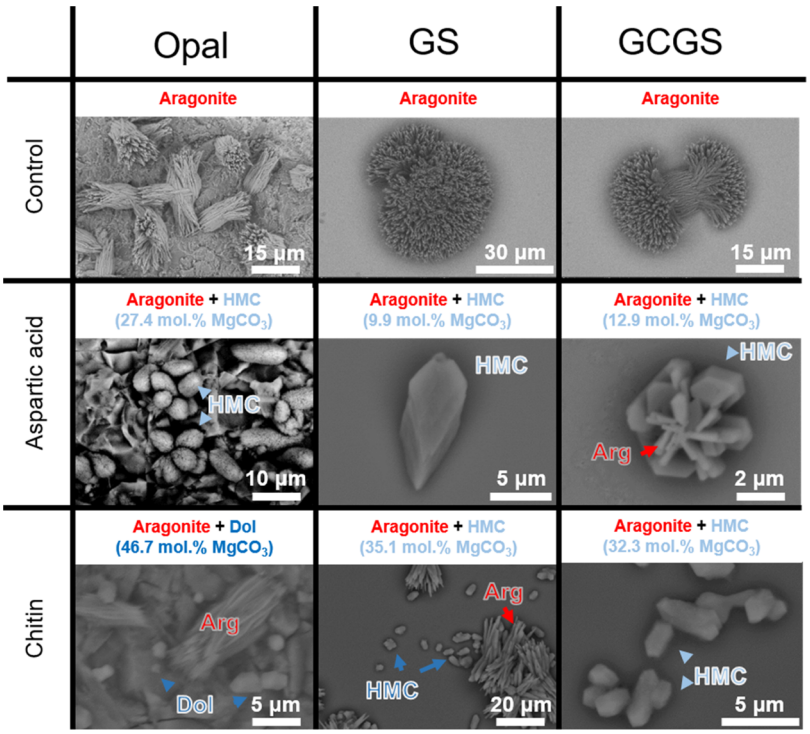

Figure 2. SEM images of precipitates on opal, glass slide (GS), and gold-coated glass slide (GCGS) surfaces in control, aspartic acid, and chitin experiments showing various morphologies of Ca−Mg carbonates, such as high-Mg calcite (HMC) with the {104} and {100} crystallographic forms and disordered dolomite (Dol) and aragonite (Arg). $MgCO_3$ values are obtained from both XRD and SEM−EDS.

of the $R\bar{3}$ space group compared to the $R\bar{3}c$ space group in calcite with only *a*-reflections present. HMC crystals in chitin experiments are rhombohedral in shape with well-developed {104} crystal facies (Figure 1B), whereas precipitates from aspartic acid experiments show as bundles of elongated crystals with less regular shaped crystals (Figure 1D).

Mineralogy of Synthetic Biocarbonate Precipitates on Solid Surfaces with Organic Substrates. Upon introducing solid surfaces (opal, glass slides, and gold-coated glass slides) for the organic substrates to attach to, we observed an additional set of carbonate precipitation behaviors. XRD and SEM−EDS revealed a significant increase in the Mg content in calcium carbonate precipitates on opal surfaces compared to in solution. Precipitates from aspartic acid experiments increased from 21.8 mol % $MgCO_3$ in solution to 27.4 mol % $MgCO_3$ on opal surfaces, and chitin experiments increased from 21.9 mol % $MgCO_3$ in solution to 46.3 mol % $MgCO_3$ (disordered dolomite) on opal surfaces (Figure 2 and Table 2). Compared to opal surfaces, experiments on glass slide (GS) and gold-coated glass slide (GCGS) surfaces showed different trends between aspartic acid and chitin, where the Mg content increased in chitin experiments (32.3 mol % $MgCO_3$ on GS and 35.1 mol % $MgCO_3$ on GCGS) but decreased in aspartic acid experiments (9.9 mol % $MgCO_3$ on GS and 12.9 mol % $MgCO_3$ on GCGS) compared to precipitates in solution (Table 2). Aragonite was present in all solid precipitation experiments.

SEM images demonstrated that precipitates have different crystal sizes and morphologies on opal, GS, and GCGS surfaces (Figure 2). In aspartic acid experiments, HMC forms as elongated spherulites on opal surfaces form (~10 μm) and as euhedral crystals on GS (~5 μm) and GCGS (~2 μm; Figure 2). In chitin experiments, disordered dolomite precipitates as 1−3 μm (smaller based on TEM image) sized euhedral crystals with the {104} crystallographic form on opal surfaces while HMC forms as slightly more elongated euhedral crystals with both the {104} and {100} forms on GS and GCGS surfaces (Figure 2). Aragonite spherulites precipitated on all three surfaces with a slower growth rate on the opal surface (Figure 2). Electron backscatter diffraction (EBSD) revealed that precipitates on GCGS surfaces displayed a strong preferred crystallographic orientation with the *c*-axes perpendicular to the surface, while the preferred orientation was diminished on GS surfaces (Figure 3). Twinning is only observed in precipitates from solution in aspartic acid experiments (HMC with (012) twins) but not in chitin experiments (Figure S1).

A series of Raman spectra and optical images reveal a transformation from magnesium-rich amorphous calcium carbonate (Mg ACC) to HMC precipitates in the glass slide aspartic acid experiments. The Mg ACC phases were still present approximately six months after being precipitated (Figure 4A). We assume that these are Mg ACC spectra due to the very wide full width at half-maximum (FWHM) of the ν_1 carbonate group symmetric stretching vibrational mode peak, which signals increased disorder and also resembles the shape of the lower-Mg ACC standard (Figure 4A,C). It is important to note that wider FWHMs can also be a function of smaller particle sizes, but this is not likely the case here because we still observe wide FWHM in spectra collected off of single crystals. As the precipitates transformed from Mg ACC to become more like HMC, the ν_1 mode peaks became thinner and sharper (Figure 4C). We also observed that the Raman water envelope (~3500 cm^{-1}) for Mg ACC (Figure 4A, spectra E−G) resembled the reference low-Mg ACC standard and began to disappear in the crystal, which appeared to be transforming

https://doi.org/10.1021/acs.cgd.3c00102
Cryst. Growth Des. 2023, 23, 4872−4882

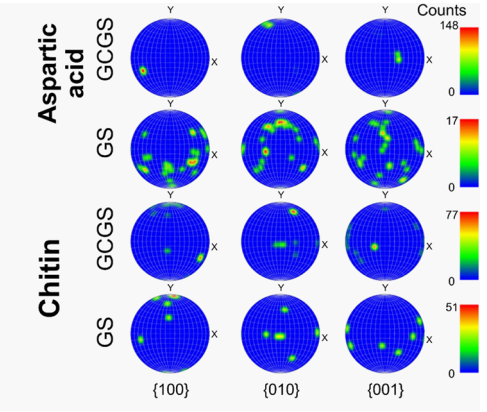

Figure 3. EBSD pole figures showing a strong preferred crystallographic orientation of high-Mg calcite (HMC) on gold-coated glass slide (GCGS) surfaces and a lesser degree of preferred orientation on the glass slide (GS) surfaces from aspartic acid and chitin experiments.

to a more anhydrous HMC-like structure (Figure 4A, spectrum H). The high Mg content in these precipitates is observable via Raman by how the ν_1 vibrational mode is shifted toward higher frequencies compared to a low-Mg natural calcite sample, but not as high as a natural dolomite sample (Figure 4C).[33]

DISCUSSION

Despite extensive works on the effects of amino acids on the calcium carbonate system,[34−37] the effects of amino acids and chitins on Ca−Mg carbonate crystallization are poorly constrained. This work provides an overview of the effects of amino acids and chitins on Ca−Mg carbonate mineralogy, composition, and morphology in both solutions and on solid surfaces via *in vitro* experiments.

Acidic Amino Acids and Chitin Enable Mg Incorporation into Calcium Carbonate. Previous studies have demonstrated that acidic proteins promote calcium carbonate nucleation when on solid templates and inhibit crystal growth in solution.[27,38−41] In nature, acidic proteins are commonly associated with the biomineralization of carbonates that make up shells, skeletons, and spicules.[5,26,42] Aspartic acids in particular were shown to modify calcite crystal morphology by altering the surface energy at certain crystallographic facies.[37,43−45] As a consequence, aspartic acid exerts a strong influence on crystal morphology.[46] Chitin also wields a significant influence on ACC and calcium carbonate growth.[47,48] Chitin is known to be widespread in biocalcifiers

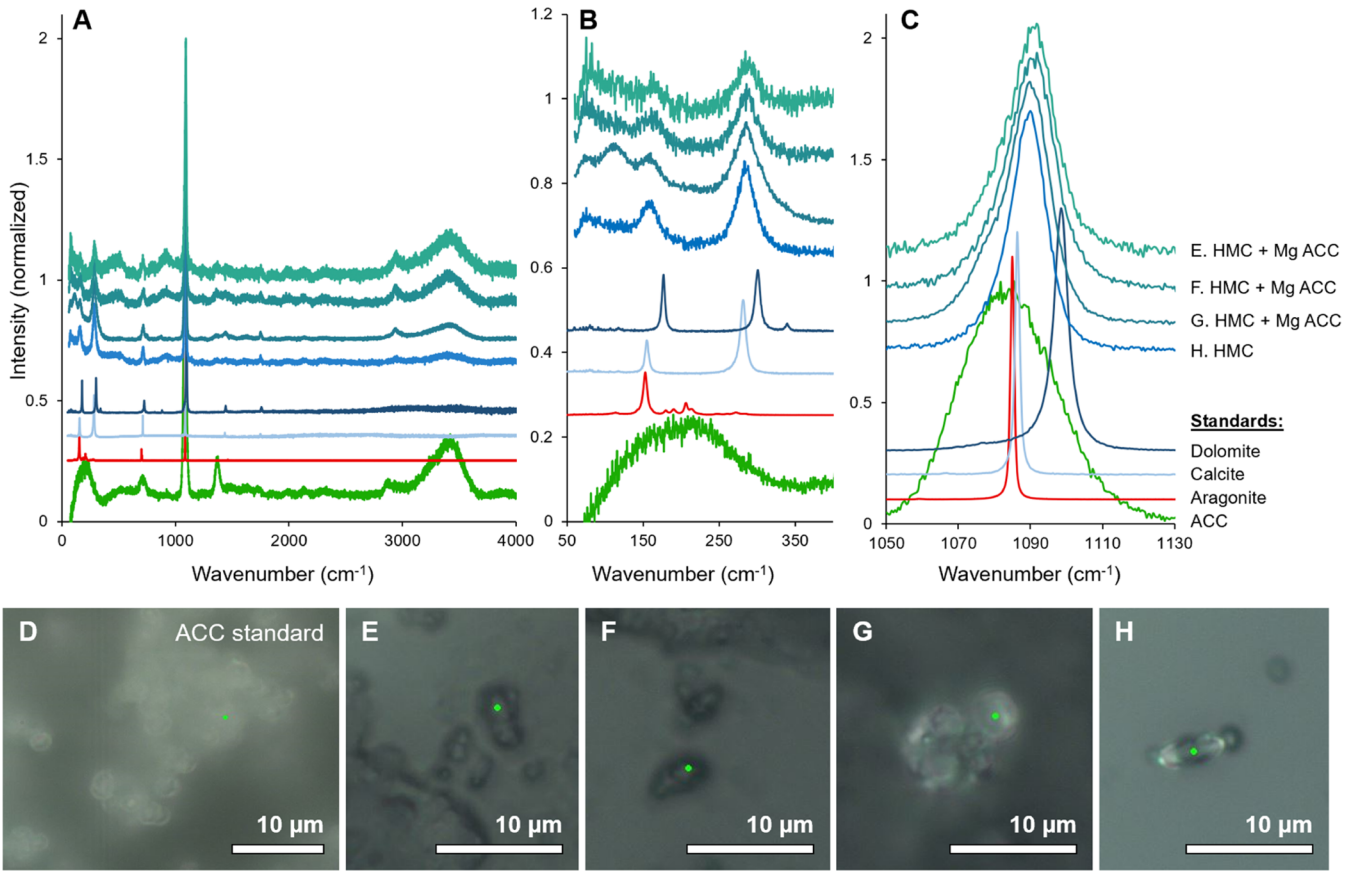

Figure 4. Raman spectroscopy measurements of Mg-rich amorphous calcium carbonate (Mg ACC) to high-Mg calcite (HMC) transformations in precipitates from the aspartic acid on glass slide experiments, compared to carbonate standards. (A) Full spectra from 20 to 4000 cm^{-1}. Zoomed-in spectra featuring (B) low-wavenumber internal modes, such as translational and librational modes between 50 and 400 cm^{-1}, and (C) v_1 symmetric stretching mode between 1050 and 1130 cm^{-1}. Peak positions for the major carbonate modes in this sample fall between peak positions for calcite (light blue) and dolomite (dark blue) standards and have FWHMs that fall between the range for the low-Mg ACC example and the crystalline carbonate mineral standards. Photomicrographs in reflected light show where spectra were collected from (D) an Mg ACC example grown on a gold-coated glass slide aspartic acid experiment sample, and (E−H) ACC-to-HMC transformations in the glass slide aspartic acid sample.

https://doi.org/10.1021/acs.cgd.3c00102
Cryst. Growth Des. 2023, 23, 4872−4882

and likely contributes to the formation of calcium carbonates in coralline algae,[49,50] crustaceans,[51] ostracods,[52] and mollusks.[53] Laboratory experiments have also demonstrated that chitin has the ability to promote heterogeneous nucleation of calcite at room temperature without the presence of magnesium.[54,55]

Mg incorporation in calcite-structure carbonates is difficult at Earth surface conditions due to the high kinetic barrier from strong Mg−water complexing that prevents Mg from bonding with CO_3^{2-}.[17,18,56] This constitutes part of the famous "dolomite problem", where the formation of massive deposits of dolomite in the geologic past cannot be explained by modern surface geological processes. Previous experiments demonstrated that catalysts such as dioxane,[57] carboxylated polystyrene,[58] dissolved silica,[19] ethanol,[17] hydrogen sulfide,[20] polysaccharide,[21] and exopolymeric substances (EPS; 21) could promote the Mg−water complex to dehydrate at ambient conditions and allow for Mg to incorporate into the calcite structure. This study demonstrates that only acidic, hydrophilic, and negatively charged polar amino acids, such as Asp and Glu, are able to catalyze Mg−water dehydration and promote anhydrous Mg-bearing carbonate precipitation, while glycine, serine, phenylalanine, leucine, and isoleucine solutions only precipitated aragonite (Figure 1 and Table 1). Previous synthesis experiments also established that aspartic acid could destabilize ACC and crystallize to calcite in the presence of magnesium in the solution.[59]

Increasing the aspartic acid concentration further enhances Mg incorporation into carbonate, similar to the behavior of other catalysts (Figure 5A; 16, 18−20). Higher initial Mg concentration in solutions will also result in higher Mg incorporation (Figure 5B). Our findings demonstrate that Asp, Glu, and chitin, in solution, have similar effects as all other catalysts in promoting Mg−water dehydration, increasing Mg incorporation into the calcite-structure carbonate, and inhibiting aragonite precipitation.

The ability to catalyze Ca−Mg carbonate precipitation with these organic molecules might be comparable to absorbed ethanol. It has been shown previously that adsorbed ethanol on carbonate surfaces produces a hydrophobic layer, retarding the calcium carbonate precipitation rate,[60] disrupting the Mg hydration shell, and promoting Ca−Mg carbonate formation.[17] It has also been postulated that acidic amino acids can regulate calcium ions through carboxylate side chains, which may also serve as a way to feed Mg into the calcite structure.[61,62] Aspartic acid is suggested to have a stronger inhibiting effect than glutamic acid in solution on calcium carbonate crystallization.[62] This difference in capacity in regulating calcium carbonate precipitation stems from the slight variance in geometry and larger space that allows the carboxylate group in aspartic acids to bind with multiple calcium ions, while glutamic acid can only bind to fewer cations.[62] However, we do not observe a clear difference in the Mg contents of Ca−Mg carbonate precipitates between aspartic acid and glutamic acid experiments (Table 1), which is likely a result of magnesium being a much smaller cation compared to calcium and resulting in no preferential binding at the carboxylate group between the two acidic amino acids. This nonpreferential binding at the carboxylate group was also observed in prior work on amorphous mineral transformation kinetics.[59]

Ca−Mg carbonate crystals precipitated with aspartic acid and chitin on solid surfaces have significantly different behaviors in both composition and morphology, suggesting a

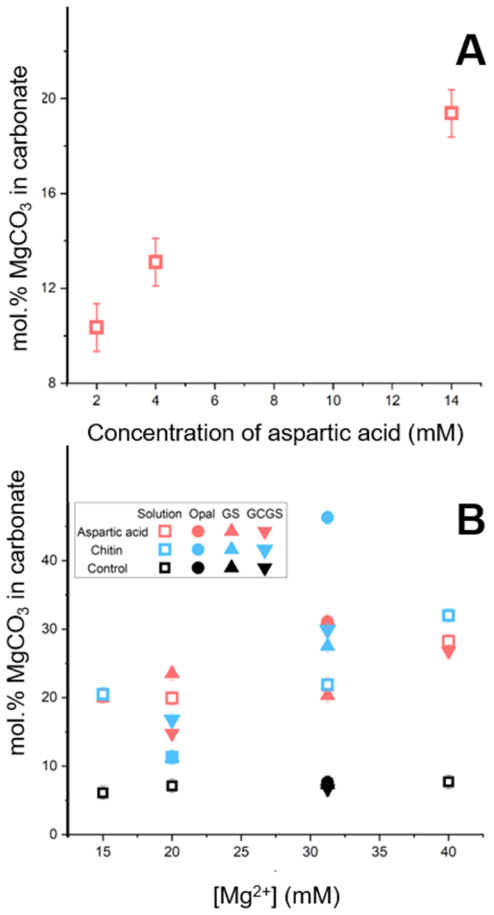

Figure 5. (A) Mole percent of $MgCO_3$ in carbonates precipitated from the solution increases with increasing aspartic acid concentrations with $[Ca^{2+}]$ = 10 mM, $[Mg^{2+}]$ = 20 mM, and $[CO_3^{2-}]$ = 40 mM. (B) Mole percent of $MgCO_3$ in carbonates precipitated from solutions and on solid surfaces (opal, GCGS, and GS). Results are compared for aspartic acid (14 mM, red symbols), chitin (0.0375 g/L, blue symbols), and control (no added biosubstrates, black symbols) experiments. Experiments with aspartic acid and chitin positively correlated with increasing $[Mg^{2+}]$ in the initial solution ($[Ca^{2+}]$ = 10 mM, $[CO_3^{2-}]$ = 40 mM).

different crystallization mechanism when organic catalysts are absorbed onto solid surfaces. Previous works in pure calcium carbonate systems propose that acidic amino acids[63] and chitin[55] would promote heterogeneous nucleation and inhibit homogeneous nucleation in solution. We observe elevated Mg incorporation in Ca−Mg carbonate precipitates in both solution and solid surface experiments with aspartic acid and chitin, although Mg tends to be more elevated in solid surface experiments (Table 2). The exception is the reduced Mg content in Asp experiments on GS and GCGS surfaces. The strongest effect we observed was chitin on opal surfaces, resulting in disordered dolomite nucleation and growth, suggesting a stronger catalytic effect than chitin in solution or amino acid induced heterogeneous nucleation (Figures 1 and 2). It is possible that the high surface area and regular distribution of the nanospheres on the freshly broken opal-A surface might have contributed to Ca−Mg carbonate nucleation in a manner similar to clay mineral surfaces.[64,65]

Being a polysaccharide could also explain chitin's ability to promote HMC and disordered dolomite precipitation, since some polysaccharides (carboxymethyl cellulose and agar) were

https://doi.org/10.1021/acs.cgd.3c00102
Cryst. Growth Des. 2023, 23, 4872−4882

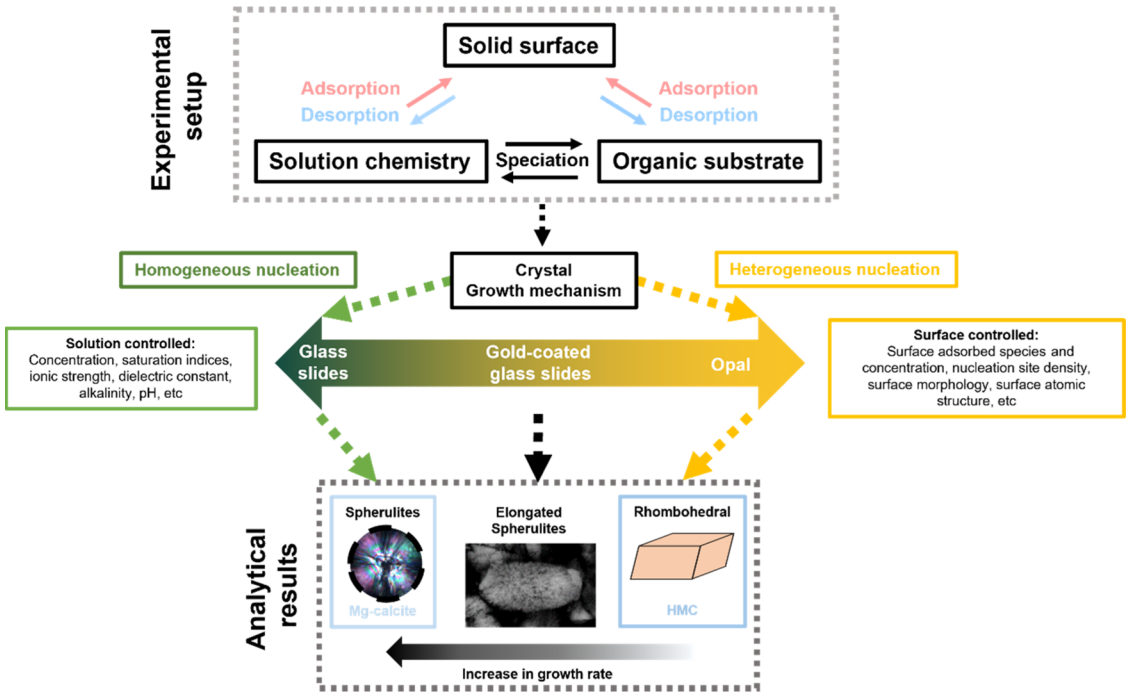

Figure 6. Schematic showing various factors controlling morphology and growth rate of carbonate minerals. For more detail on crystal morphologies, see Figures S2 and S3. Here we connect spherulitic growth associated with faster growth rates and lower Mg concentrations with solution-controlled systems that depend primarily on solution chemistry, whereas the euhedral crystal morphologies (that are also more Mg-rich) align best with surface controlled conditions where organic substrates and solid surfaces play a larger role.

shown to catalyze disordered dolomite formation in the laboratory.[21]

Raman spectroscopy measurements on solid surface precipitates reveal the presence of amorphous calcium carbonate (ACC), known to stay preserved in this form in abiogenic settings with increased Mg content.[66] This may indicate that ACC precursor phases play a role in the crystallization mechanism of the heterogeneous precipitation experiments. Numerous investigations have found that chitin induces ACC formation;[67−69] however, the transformation of Mg ACC to crystalline carbonate was not observed in the chitin solid substrate experiments in this study, at least on longer timescales (months after the experiment). We were still able to measure ACC and Mg ACC in the aspartic acid experiments after six months. This likely suggests either a different crystallization pathway between aspartic acid and chitin biosubstrates, or ACC in the chitin experiments had a substantially shorter residence time. Previous studies have demonstrated that aspartate can also stabilize $CaCO_3$ prenucleation clusters and thus potentially stabilize Mg ACC.[36,70,71]

Acidic Amino Acids and Chitin Controlling Carbonate Crystal Morphology on Solid Substrate Surfaces. It is known that organisms can control the morphology of biominerals through various approaches, such as using ACC precursor phases in echinoderms,[72] or an organic matrix framework in mollusk nacre.[73] Here, aspartic acid and chitin on solid substrate surfaces show a strong control on crystal morphology through heterogeneous nucleation (Figure 2). In the pure calcium system, it is established that chitin on exoskeleton surfaces could control calcium carbonate formation[68] and orientation.[68,74] Our study demonstrates that chitin adsorbed onto solid surfaces assumes the same role in controlling crystal orientation for HMC (Figure 3).

Since there is no evidence suggesting the presence of ACC in our chitin *in vitro* experiments, and oriented growth of Mg carbonate is only known to happen on clay, and other mineral surfaces through classical crystallization pathways,[64,65] it is likely that chitin adsorbed onto solid surfaces provides heterogeneous nucleation sites that lower the crystallization energy and Mg−water dehydration energy, resulting in oriented growth of HMC and disordered dolomite (Figures 2, 3, and 6). Although aspartic acid adsorbed surfaces show a similar trend of Mg calcite crystal-oriented growth, it is less coherent compared to chitin counterparts, indicating a weaker heterogeneous nucleation process (Figures 2 and 3). This may help to explain why some organisms utilize both acidic amino acids and chitins to control the morphology and crystal orientation of precipitated Ca−Mg carbonates during biomineralization, similar to cases for pure calcium bicarbonates.[73] In this study, we demonstrate that Asp and chitin experiments display different effects on crystal texture during heterogeneous nucleation (Figure 2). The difference in carbonate morphology on different solid substrate surfaces, i.e., opal, GS, and GCGS, could be a result of different degrees of the short-range ordering of silica tetrahedral. While the GS and GCGS are amorphous without short-range ordering, opal-A surface was shown to exhibit local six-member rings of silica tetrahedral and short-range ordering.[75] These six-member rings of silica on the surface could exert a stronger surface effect and promote heterogeneous nucleation on them.[19,64,76] In Figure 6, we outline a model of how different Ca−Mg carbonate crystal morphologies were achieved by following various homogeneous and heterogeneous nucleation pathways set up by our experiments combining solutions with organic substrates and solid surfaces. Surface-controlled (heterogeneous nucleation) pathways would result in euhedral crystals via relatively slow growth rates with higher Mg incorporation, while solution-

https://doi.org/10.1021/acs.cgd.3c00102
Cryst. Growth Des. 2023, 23, 4872−4882

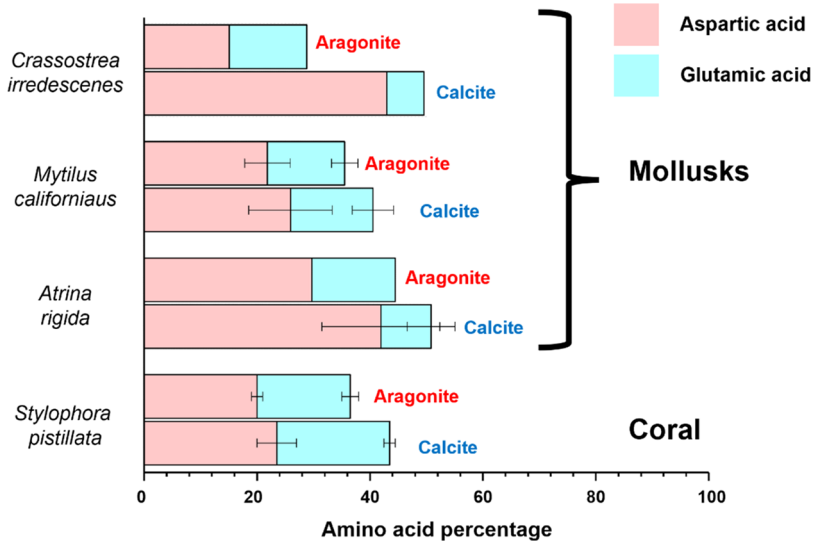

Figure 7. Compiled data showing aspartic and glutamic acid proportions in regions with calcite and with aragonite in bimineralic organisms. *Crassostrea irredescenes*,[27] *Mytilus californiaus*,[82] *Atrina rigida*,[53,81] and *Stylophora pistillate*.[4]

controlled pathways (homogeneous nucleation) would result in spherulite formation, indicating rapid growth rates.

Ca−Mg Carbonate Growth in Biomineral Systems. Despite dolomite precipitation being thermodynamically favorable, in seawater, aragonite is the predominant carbonate mineral to precipitate due to high Mg/Ca ratios and the high kinetic barrier of the Mg−water complex.[17] Thus, aragonite is a common biomineral phase used by many marine organisms, such as corals and mollusks. Still, other organisms continue to form calcite and other carbonate phases, likely with the aid of acidic proteins and chitins that have been shown to promote the precipitation of calcite-structure minerals in coccoliths,[77] mollusks,[78] and sea urchins.[79] In addition to their acidic properties, proteins made up of negatively charged amino acids, such as aspartic acid, also appear to significantly influence calcium carbonate formation.[36,46] The ability to drive calcite-structure mineral precipitation over aragonite via amino acid substrates is likely similar to other catalysts that drive Mg incorporation into calcite-structure carbonates, such as dissolved silica.[19,80] In this study, HMC grown on GCGS surfaces with chitin substrates has similar euhedral morphologies, preferred crystal orientations, and Mg compositions to Ca−Mg carbonates formed on the chitin-rich exoskeletons of leaf-cutter ants[7] (Figure S2). This suggests that a combination of organic substrates and solid surface properties may control calcite structure formation and Mg incorporation via biomineralization in nature. The appearance of (012) twinning in the HMC in aspartic acid experiments is also commonly observed in modern Ca−Mg carbonates in natural abiotic settings.[31,76]

By comparing the mineralogy of biocarbonates and the composition of amino acids reported in the literature, we observe that organisms that utilize both aragonite and calcite in their hard parts (skeletons, shells, etc.) have higher Asp and Glu content in the calcitic regions and lower acidic amino acid contents in the aragonitic regions[4,27,49,73,74] (Figure 7). This supports our hypothesis that many biomineralizing organisms likely control their mineralogy, crystal chemistry, and crystal morphology by mixing different organic substrate catalysts to precipitate specific calcium carbonate minerals. Understanding these combinations and subsequent precipitates could have implications for forming synthetic biomimetic materials in the future, especially ones with higher Mg contents and improved material properties.

Compared to those that produce pure Ca carbonates, biomineralizing organisms that produce Ca−Mg carbonates may hold added benefits, such as lower dissolution rates when the Mg content reaches at least ∼40 mol %, higher Mohs hardness, and a greater potential for carbon sequestration. Leaf-cutter ants, which were recently shown to form Ca−Mg carbonate on their chitin-rich exoskeletons, may take advantage of this by using harder carbonates as armor,[7] as well as a robust mineral-based carbon sink to reduce the extremely high pCO_2 (up to 3 vol %) in their colonies.[83] Using a closed box mass balance model, we roughly estimate that a colony with 8 million ants forming a 1 μm thick layer of Ca−Mg carbonates on their exoskeletons could sequester up to 5−10% of the carbon dioxide in the colony in this solid form (Supporting Information). In contrast to a 50:50 Ca/Mg carbonate phase, using the same amount of Ca^{2+} available on the ant exoskeletons, precipitation of a pure calcium end-member would provide half the carbon sequestration potential and face more significant dissolution from the low pH environment in the ant colony. This demonstrates that Ca−Mg carbonate biominerals may serve as a much more practical carbon sequestration agent in the biosphere.

■ CONCLUSIONS

Our results demonstrate that acidic, negatively charged, hydrophilic amino acids and chitin polysaccharides can act as catalysts to dehydrate local mineral surfaces to allow Ca−Mg carbonate precipitation. Different combinations of organic substrates and solid surfaces create various crystal morphologies in experimental biomineral analogues, some of which resemble natural HMC/disordered dolomite crystals on ant exoskeletons. The ability of Mg-bearing calcium carbonates to sequester carbon, resist ocean acidification, and form harder mineral parts in biominerals offers a largely untapped reservoir of information on substrate-controlled biomineralization mechanisms, biomimetic materials synthesis, and carbon dioxide and ocean acidification mitigation responses.

https://doi.org/10.1021/acs.cgd.3c00102
Cryst. Growth Des. 2023, 23, 4872−4882

■ ASSOCIATED CONTENT

Supporting Information

The Supporting Information is available free of charge at https://pubs.acs.org/doi/10.1021/acs.cgd.3c00102.

(A) TEM image of (012) twinning of high-magnesium calcites (HMC) close to the [100] zone axis; (B) selected-area electron diffraction (SAED) pattern of (A) showing two sets of diffraction patterns, which are labeled in yellow and white; (C) crystal form models from of (012) twinning of HMC close to the [100] zone axis with same traces labeled as (A); (D) crystal form models from of (012) twinning of HMC along the [100] zone axis (Figure S1); (A) backscattered (BSE) image of synthetic quasi-rhombohedral HMC on a gold-coated glass slide surface in the chitin experiment; (B) BSE image of rhombohedral-shaped HMC on a leaf-cutter ant exoskeleton;[7] (C) BSE image of a synthetic HMC spherulite from a chitin solution experiment; (D) euhedral shape of HMC with {104} and {100} crystallographic forms; (E) ideal shape of rhombohedral HMC with only {104} faces developed (Figure S2); (A) cross-polarized light image of Mg-calcite spherulites growing from solution in chitin experiments; (B) BSE image of elongated HMC spherulites growing on an opal surface in the aspartic acid experiment; (C) euhedral HMC growing on a GCGS surface in the chitin experiment (Figure S3); box model for estimating CO_2 sequestration via dolomite precipitation ($CaMg(CO_3)_2$) in an ant colony (Figure S4); and results of *in vitro* experiments with aspartic acid, chitin, and no organic substrates (Table S1); *denotes a minor amount (PDF)

■ AUTHOR INFORMATION

Corresponding Authors

Yihang Fang − *Department of Geoscience, University of Wisconsin-Madison, Madison, Wisconsin 53706, United States; Department of Mineral Sciences, National Museum of Natural History, Smithsonian Institution, Washington, District of Columbia 20560, United States; Department of Earth and Planetary Sciences, Washington University in St. Louis, St. Louis, Missouri 63130, United States;* orcid.org/0000-0002-8218-5883; Email: yihang@wustl.edu

Gabriela A. Farfan − *Department of Mineral Sciences, National Museum of Natural History, Smithsonian Institution, Washington, District of Columbia 20560, United States;* orcid.org/0000-0001-5204-7044; Email: farfang@si.edu

Authors

Seungyeol Lee − *USRA Lunar and Planetary Institute, Houston, Texas 77058, United States; ARES, NASA Johnson Space Center, Houston, Texas 77058, United States; Department of Earth and Environmental Sciences, Chungbuk National University, Cheongju 28644, Republic of Korea;* orcid.org/0000-0002-0175-1389

Huifang Xu − *Department of Geoscience, University of Wisconsin-Madison, Madison, Wisconsin 53706, United States;* orcid.org/0000-0002-7464-0057

Complete contact information is available at: https://pubs.acs.org/10.1021/acs.cgd.3c00102

Notes

The authors declare no competing financial interest.

■ ACKNOWLEDGMENTS

The authors would like to thank the Smithsonian Institution Big Ten Alliance Fellowship for supporting this work, and Paul Pohwat for help with selecting mineral standards from the Smithsonian National Gem and Mineral Collection. They appreciate the constructive comments from the three anonymous reviewers and Dr. Jeffrey Rimer for handling this manuscript and would also like to thank Bil Schneider for his assistance with the SEM and EBSD measurements.

■ REFERENCES

(1) Knoll, A. H. Biomineralization and Evolutionary History. *Rev. Mineral. Geochem.* **2003**, *54*, 329−356.

(2) Langer, G.; Geisen, M.; Baumann, K. H.; Kläs, J.; Riebesell, U.; Thoms, S.; Young, J. R. Species-Specific Responses of Calcifying Algae to Changing Seawater Carbonate Chemistry. *Geochem., Geophys. Geosystems* **2006**, *7*, No. 01227.

(3) Schiebel, R. Planktic Foraminiferal Sedimentation and the Marine Calcite Budget. *Global Biogeochem. Cycles* **2002**, *16*, 3-1−3-21.

(4) Mass, T.; Drake, J. L.; Haramaty, L.; Rosenthal, Y.; Schofield, O. M. E.; Sherrell, R. M.; Falkowski, P. G. Aragonite Precipitation by "Proto-Polyps" in Coral Cell Cultures. *PLoS One* **2012**, *7*, No. e35049.

(5) Addadi, L.; Joester, D.; Nudelman, F.; Weiner, S. Mollusk Shell Formation: A Source of New Concepts for Understanding Biomineralization Processes. *Chem. - Eur. J.* **2006**, *12*, 980−987.

(6) Weber, J.; Greer, R.; Voight, B.; White, E.; Roy, R. Unusual Strength Properties of Echinoderm Calcite Related to Structure. *J. Ultrastruct. Res.* **1969**, *26*, 355−366.

(7) Li, H.; Sun, C. Y.; Fang, Y.; Carlson, C. M.; Xu, H.; Ješovnik, A.; Sosa-Calvo, J.; Zarnowski, R.; Bechtel, H. A.; Fournelle, J. H.; Andes, D. R.; Schultz, T. R.; Gilbert, P. U. P. A.; Currie, C. R. Biomineral Armor in Leaf-Cutter Ants. *Nat. Commun.* **2020**, *11*, No. 5792.

(8) Rangarajan, R.; Ghosh, P.; Naggs, F. Seasonal Variability of Rainfall Recorded in Growth Bands of the Giant African Land Snail Lissachatina Fulica (Bowdich) from India. *Chem. Geol.* **2013**, *357*, 223−230.

(9) Mann, S.; Parker, S. B.; Ross, M. D.; Skarnulis, A. J.; Williams, R. J. The Ultrastructure of the Calcium Carbonate Balance Organs of the Inner Ear: An Ultra-High Resolution Electron Microscopy Study. *Proc. R. Soc. London, Ser. B* **1983**, *218*, 415−424.

(10) Ridgwell, A.; Zeebe, R. E. The Role of the Global Carbonate Cycle in the Regulation and Evolution of the Earth System. *Earth Planet. Sci. Lett.* **2005**, *234*, 299−315.

(11) Gilbert, P.; Bergmann, K.; Boekelheide, N.; Tambutté, S.; Mass, T.; Marin, F.; Adkins, J. F.; Gilbert, B.; Knutson, V.; Cantine, M.; Hernández, J. O.; Knoll, A. H. Biomineralization: Integrating Mechanism and Evolutionary History. *Sci. Adv.* **2021**, *8*, No. eabl9653.

(12) Doney, S. C.; Fabry, V. J.; Feely, R. A.; Kleypas, J. A. Ocean Acidification: The Other CO_2 Problem. *Annu. Rev. Mar. Sci.* **2009**, *1*, 169−192.

(13) Nash, M. C.; Uthicke, S.; Negri, A. P.; Cantin, N. E. Ocean Acidification Does Not Affect Magnesium Composition or Dolomite Formation in Living Crustose Coralline Algae, Porolithon Onkodes in an Experimental System. *Biogeosciences* **2015**, *12*, 5247−5260.

(14) Tanaka, S.; Hatano, H.; Itasaka, O. Biochemical Studies on Pearl. VIII. Occurence of Calcite, Aragonite and Dolomite in Pearl and Shell. *Bull. Chem. Soc. Jpn.* **1960**, *33*, 182−185.

(15) Zhou, C.; Jin, S.; Sun, Z.; Homkrajae, A.; Myagkaya, E.; Nilpetploy, N.; Lawanwong, K. Disordered dolomite as an unusual biomineralization product found in the center of a natural *Cassis* pearl. *PLOS ONE* **2023**, *18*, e0284295.

(16) Ma, Y.; Aichmayer, B.; Paris, O.; Fratzl, P.; Meibom, A.; Metzler, R. A.; Politi, Y.; Addadi, L.; Gilbert, P. U. P. A.; Weiner, S.

The Grinding Tip of the Sea Urchin Tooth Exhibits Exquisite Control over Calcite Crystal Orientation and Mg Distribution. *Proc. Natl. Acad. Sci. U.S.A.* **2009**, *106*, 6048−6053.
(17) Fang, Y.; Zhang, F.; Farfan, G. A.; Xu, H. Low-Temperature Synthesis of Disordered Dolomite and High-Magnesium Calcite in Ethanol−Water Solutions: The Solvation Effect and Implications. *ACS Omega* **2022**, *7*, 281−292.
(18) Lippmann, F. The Polymorphism Calcite-Aragonite. In *Sedimentary Carbonate Minerals*; Springer: New York, 1973.
(19) Fang, Y.; Xu, H. Dissolved Silica-Catalyzed Disordered Dolomite Precipitation. *Am. Mineral.* **2022**, *107*, 443−452.
(20) Zhang, F.; Xu, H.; Konishi, H.; Kemp, J. M.; Roden, E. E.; Shen, Z. Dissolved Sulfide-Catalyzed Precipitation of Disordered Dolomite: Implications for the Formation Mechanism of Sedimentary Dolomite. *Geochim. Cosmochim. Acta* **2012**, *97*, 148−165.
(21) Zhang, F.; Xu, H.; Konishi, H.; Shelobolina, E. S.; Roden, E. E. Polysaccharide-Catalyzed Nucleation and Growth of Disordered Dolomite: A Potential Precursor of Sedimentary Dolomite. *Am. Mineral.* **2012**, *97*, 556−567.
(22) Zhang, F.; Xu, H.; Shelobolina, E. S.; Konishi, H.; Converse, B.; Shen, Z.; Roden, E. E. The Catalytic Effect of Bound Extracellular Polymeric Substances Excreted by Anaerobic Microorganisms on Ca-Mg Carbonate Precipitation: Implications for the "Dolomite Problem.". *Am. Mineral.* **2015**, *100*, 483−494.
(23) Zhang, F.; Xu, H.; Shelobolina, E. S.; Konishi, H.; Roden, E. E. Precipitation of Low-Temperature Disordered Dolomite Induced by Extracellular Polymeric Substances of Methanogenic Archaea Methanosarcina Barkeri: Implications for Sedimentary Dolomite Formation. *Am. Mineral.* **2021**, *106*, 69−81.
(24) Treves, K.; Traub, W.; Weiner, S.; Addadi, L. Aragonite Formation in the Chiton (Mollusca) Girdle. *Helv. Chim. Acta* **2003**, *86*, 1101−1112.
(25) Weiner, S.; Erez, J. Organic Matrix of the Shell of the Foraminifer, Heterostegina Depressa. *J. Foraminiferal Res.* **1984**, *14*, 206−212.
(26) Mass, T.; Drake, J. L.; Peters, E. C.; Jiang, W.; Falkowski, P. G. Immunolocalization of Skeletal Matrix Proteins in Tissue and Mineral of the Coral Stylophora Pistillata. *Proc. Natl. Acad. Sci. U.S.A.* **2014**, *111*, 12728−12733.
(27) Weiner, S.; Hood, L. Soluble Protein of the Organic Matrix of Mollusk Shells: A Potential Template for Shell Formation. *Science* **1975**, *190*, 987−989.
(28) Weiner, S.; Traub, W. Macromolecules in Mollusc Shells and Their Functions in Biomineralization. *Philos. Trans. R. Soc., B* **1984**, *304*, 425−434.
(29) Albeck, S.; Weiner, S.; Addadi, L. Polysaccharides of Intracrystalline Glycoproteins Modulate Calcite Crystal Growth in Vitro. *Chem. - Eur. J.* **1996**, *2*, 278−284.
(30) Zhang, F.; Xu, H.; Konishi, H.; Roden, E. E. A Relationship between d_{104} Value and Composition in the Calcite-Disordered Dolomite Solid-Solution Series. *Am. Mineral.* **2010**, *95*, 1650−1656.
(31) Fang, Y.; Xu, H. A New Approach to Quantify the Ordering State of Protodolomite Using Xrd, Tem, and z-Contrast Imaging. *J. Sediment. Res.* **2019**, *89*, 537−551.
(32) Fang, Y.; Xu, H. A New Approach to Quantify Ordering State of Protodolomite Using XRD, TEM, and Z-Contrast Imaging. *J. Sediment. Res.* **2019**, *89*, 537−551.
(33) Perrin, J.; Vielzeuf, D.; Laporte, D.; Ricolleau, A.; Rossman, G. R.; Floquet, N. Raman Characterization of Synthetic Magnesian Calcites. *Am. Mineral.* **2016**, *101*, 2525−2538.
(34) Müller, P. J.; Suess, E. Interaction of Organic Compounds with Calcium Carbonate-III. Amino Acid Composition of Sorbed Layers. *Geochim. Cosmochim. Acta* **1977**, *41*, 941−949.
(35) Suess, E. Interaction of Organic Compounds with Calcium Carbonate-I. Association Phenomena and Geochemical Implications. *Geochim. Cosmochim. Acta* **1970**, *34*, 157−168.
(36) Picker, A.; Kellermeier, M.; Seto, J.; Gebauer, D.; Cölfen, H. The Multiple Effects of Amino Acids on the Early Stages of Calcium Carbonate Crystallization. *Z. Kristallogr. - Cryst. Mater.* **2012**, *227*, 744−757.
(37) Teng, H. H.; Dove, P. M. Surface Site-Specific Interactions of Aspartate with Calcite during Dissolution: Implications for Biomineralization. *Am. Mineral.* **1997**, *82*, 878−887.
(38) Stephenson, A. E.; DeYoreo, J. J.; Wu, L.; Wu, K. J.; Hoyer, J.; Dove, P. M. Peptides Enhance Magnesium Signature in Calcite: Insights into Origins of Vital Effects. *Science* **2008**, *322*, 724−727.
(39) Fu, G.; Qiu, S. R.; Orme, C. A.; Morse, D. E.; De Yoreo, J. J. Acceleration of Calcite Kinetics by Abalone Nacre Proteins. *Adv. Mater.* **2005**, *17*, 2678−2683.
(40) Elhadj, S.; De Yoreo, J. J.; Hoyer, J. R.; Dove, P. M. Role of Molecular Charge and Hydrophilicity in Regulating the Kinetics of Crystal Growth. *Proc. Natl. Acad. Sci. U.S.A.* **2006**, *103*, 19237−19242.
(41) Chen, C. L.; Qi, J.; Zuckermann, R. N.; Deyoreo, J. J. Engineered Biomimetic Polymers as Tunable Agents for Controlling $CaCO_3$ Mineralization. *J. Am. Chem. Soc.* **2011**, *133*, 5214−5217.
(42) Gilbert, P. U. P. A.; Wilt, F. H. Molecular Aspects of Biomineralization of the Echinoderm Endoskeleton. *Prog. Mol. Subcell. Biol.* **2011**, *52*, 199−223.
(43) Deoliveira, D. B.; Laursen, R. A. Control of Calcite Crystal Morphology by a Peptide Designed To Bind to a Specific Surface. *J. Am. Chem. Soc.* **1997**, *7863*, 10627−10631.
(44) Teng, H. H.; Dove, P. M.; Orme, C. A.; De Yoreo, J. J. Thermodynamics of Calcite Growth: Baseline for Understanding Biomineral Formation. *Science* **1998**, *282*, 724−727.
(45) Orme, C. A.; Noy, A.; Wierzbicki, A.; McBride, M. T.; Grantham, M.; Teng, H. H.; Dove, P. M.; DeYoreo, J. J. Formation of Chiral Morphologies through Selective Binding of Amino Acids to Calcite Surface Steps. *Nature* **2001**, *411*, 775−779.
(46) Xie, A. J.; Shen, Y. H.; Zhang, C. Y.; Yuan, Z. W.; Zhu, X. M.; Yang, Y. M. Crystal Growth of Calcium Carbonate with Various Morphologies in Different Amino Acid Systems. *J. Cryst. Growth* **2005**, *285*, 436−443.
(47) Falini, G.; Fermani, S.; Conforti, G.; Ripamonti, A. Protein Crystallisation on Chemically Modified Mica Surfaces. *Acta Crystallogr., Sect. D: Biol. Crystallogr.* **2002**, *58*, 1649−1652.
(48) Falini, G.; Weiner, S.; Addadi, L. Chitin-Silk Fibroin Interactions: Relevance to Calcium Carbonate Formation in Invertebrates. *Calcif. Tissue Int.* **2003**, *72*, 548−554.
(49) Rahman, M. A.; Halfar, J. First Evidence of Chitin in Calcified Coralline Algae: New Insights into the Calcification Process of Clathromorphum Compactum. *Sci. Rep.* **2014**, *4*, No. 6162.
(50) Rahman, M. A.; Halfar, J.; Adey, W. H.; Nash, M.; Paulo, C.; Dittrich, M. The Role of Chitin-Rich Skeletal Organic Matrix on the Crystallization of Calcium Carbonate in the Crustose Coralline Alga Leptophytum Foecundum. *Sci. Rep.* **2019**, *9*, No. 11869.
(51) Hild, S.; Marti, O.; Ziegler, A. Spatial Distribution of Calcite and Amorphous Calcium Carbonate in the Cuticle of the Terrestrial Crustaceans Porcellio Scaber and Armadillidium Vulgare. *J. Struct. Biol.* **2008**, *163*, 100−108.
(52) Rumney, B. M.; Morgan, S. R.; Mosselmans, J. F. W.; Malik, F. T.; Holden, S. J.; Parker, A. R.; White, N.; Lewis, P. N.; Albon, J.; Meek, K. M. Characterisation of Carapace Composition in Developing and Adult Ostracods (Skogsbergia Lerneri) and Its Potential for Biomaterials. *Mar. Biol.* **2022**, *169*, No. 78.
(53) Falini, G.; Albeck, S.; Weiner, S.; Addadi, L. Control of Aragonite or Calcite Polymorphism by Mollusk Shell Macromolecules. *Science* **1996**, *271*, 67−69.
(54) Manoli, F.; Koutsopoulos, S.; Dalas, E. Crystallization of Calcite on Chitin. *J. Cryst. Growth* **1997**, *182*, 116−124.
(55) Zhang, S.; Gonsalves, K. E. Influence of the Chitosan Surface Profile on the Nucleation and Growth of Calcium Carbonate Films. *Langmuir* **1998**, *14*, 6761−6766.
(56) Toroz, D.; Song, F.; Chass, G. A.; Di Tommaso, D. New Insights into the Role of Solution Additive Anions in Mg^{2+}-dehydration: Implications for Mineral Carbonation. *CrystEngComm* **2021**, *23*, 4896−4900.

https://doi.org/10.1021/acs.cgd.3c00102
Cryst. Growth Des. 2023, 23, 4872−4882

(57) Oomori, T.; Kitano, Y. Synthesis of Protodolomite from Sea Water Containing Dioxane. *Geochem. J.* **1987**, *21*, 59−65.
(58) Freire, P. T. C.; Barboza, F. M.; Lima, J. A.; Melo, F. E. A.; Filho, J. M. Raman Spectroscopy of Amino Acid Crystals. In *Raman Spectroscopy and Applications*; IntechOpen, 2017.
(59) Tao, J.; Zhou, D.; Zhang, Z.; Xu, R.; Tang, R. Magnesium-Aspartate-Based Crystallization Switch Inspired from Shell Molt of Crustacean. *Proc. Natl. Acad. Sci. U.S.A.* **2009**, *106*, 22096−22101.
(60) Cooke, D. J.; Gray, R. J.; Sand, K. K.; Stipp, S. L. S.; Elliott, J. A. Interaction of Ethanol and Water with the {10$\bar{1}$4} Surface of Calcite. *Langmuir* **2010**, *26*, 14520−14529.
(61) Weiner, S.; Traub, W. X-Ray Diffraction Study of the Insoluble Organic Matrix of Mollusk Shells. *FEBS Lett.* **1980**, *111*, 311−316.
(62) Lemke, T.; Edte, M.; Gebauer, D.; Peter, C. Three Reasons Why Aspartic Acid and Glutamic Acid Sequences Have a Surprisingly Different Influence on Mineralization. *J. Phys. Chem. B* **2021**, *125*, 10335−10343.
(63) Sikes, C. S.; Yeung, M. L.; Wheeler, A. P. Inhibition of Calcium Carbonate and Phosphate Crystallization by Peptides Enriched in Aspartic Acid and Phosphoserine. In *Surface Reactive Peptides and Polymers*, ACS Symposium Series; ACS Publications, 1991; pp 50−71.
(64) Xu, H.; Zhou, M.; Fang, Y.; Teng, H. H. Effect of Mica and Hematite (001) Surfaces on the Precipitation of Calcite. *Minerals* **2018**, *8*, No. 17.
(65) Liu, D.; Xu, Y.; Papineau, D.; Yu, N.; Fan, Q.; Qiu, X.; Wang, H. Experimental Evidence for Abiotic Formation of Low-Temperature Proto-Dolomite Facilitated by Clay Minerals. *Geochim. Cosmochim. Acta* **2019**, *247*, 83−95.
(66) Blue, C. R.; Giuffre, A.; Mergelsberg, S.; Han, N.; De Yoreo, J. J.; Dove, P. M. Chemical and Physical Controls on the Transformation of Amorphous Calcium Carbonate into Crystalline $CaCO_3$ Polymorphs. *Geochim. Cosmochim. Acta* **2017**, *196*, 179−196.
(67) Falini, G.; Fermani, S.; Ripamonti, A. Crystallization of Calcium Carbonate Salts into Beta-Chitin Scaffold. *J. Inorg. Biochem.* **2002**, *91*, 475−480.
(68) Keene, E. C.; Evans, J. S.; Estroff, L. A. Silk Fibroin Hydrogels Coupled with the n16N-β-Chitin Complex: An in Vitro Organic Matrix for Controlling Calcium Carbonate Mineralization. *Cryst. Growth Des.* **2010**, *10*, 5169−5175.
(69) Ma, Y.; Feng, Q. A Crucial Process: Organic Matrix and Magnesium Ion Control of Amorphous Calcium Carbonate Crystallization on β-Chitin Film. *CrystEngComm* **2015**, *17*, 32−39.
(70) Demichelis, R.; Raiteri, P.; Gale, J. D.; Quigley, D.; Gebauer, D. Stable Prenucleation Mineral Clusters Are Liquid-like Ionic Polymers. *Nat. Commun.* **2011**, *2*, No. 590.
(71) Zou, Z.; Bertinetti, L.; Politi, Y.; Fratzl, P.; Habraken, W. J. E. M. Control of Polymorph Selection in Amorphous Calcium Carbonate Crystallization by Poly(Aspartic Acid): Two Different Mechanisms. *Small* **2017**, *13*, No. 1603100.
(72) Beniash, E.; Aizenberg, J.; Addadi, L.; Weiner, S. Amorphous Calcium Carbonate Transforms into Calcite during Sea Urchin Larval Spicule Growth. *Proc. R. Soc. London, Ser. B* **1997**, *264*, 461−465.
(73) Veis, A. Mineralization in Organic Matrix Frameworks. *Rev. Mineral. Geochem.* **2003**, *54*, 249−289.
(74) Al-Sawalmih, A.; Li, C.; Siegel, S.; Fabritius, H.; Yi, S.; Raabe, D.; Fratzl, P.; Paris, O. Microtexture and Chitin/Calcite Orientation Relationship in the Mineralized Exoskeleton of the American Lobster. *Adv. Funct. Mater.* **2008**, *18*, 3307−3314.
(75) Lee, S.; Xu, H.; Xu, H.; Division, E. S. Reexamination of the Structure of Opal-A: A Combined Study of Synchrotron X-Ray Diffraction and Pair Distribution Function Analysis. *Am. Mineral.* **2021**, *107*, 1353−1360.
(76) Fang, Y.; Hobbs, F.; Yang, Y.; Xu, H. Dissolved Silica Driven Dolomite Precipitation in the Great Salt Lake, Utah and Its Implication for Hypersaline/Saline Environments. *Sedimentology* **2023**, No. 13081.
(77) Didymus, J. M.; Oliver, P.; Mann, S.; Arthur, L.; Hauschka, P. V.; Westbroek, P. Influence of Low-Molecular-Weight and Macromolecular Organic Additives on the Morphology of Calcium Carbonate. *J. Chem. Soc., Faraday Trans.* **1993**, *89*, 2891−2900.
(78) Suzuki, M.; Saruwatari, K.; Kogure, T.; Yamamoto, Y.; Nishimura, T.; Kato, T.; Nagasawa, H. An Acidic Matrix Protein, Pif, Is a Key Macromolecule for Nacre Formation. *Science* **2009**, *325*, 1388−1390.
(79) Albeck, S.; Aizenberg, J.; Addadi, L.; Weiner, S. Interactions of Various Skeletal Intracrystalline Components with Calcite Crystals. *J. Am. Chem. Soc.* **1993**, *115*, 11691−11697.
(80) Lakshtanov, L. Z.; Stipp, S. L. S. Interaction between Dissolved Silica and Calcium Carbonate: 1. Spontaneous Precipitation of Calcium Carbonate in the Presence of Dissolved Silica. *Geochim. Cosmochim. Acta* **2010**, *74*, 2655−2664.
(81) Gotliv, B. A.; Addadi, L.; Weiner, S. Mollusk Shell Acidic Proteins: In Search of Individual Functions. *ChemBioChem* **2003**, *4*, 522−529.
(82) Weiner, S. Mollusk Shell Formation: Isolation of Two Organic Matrix Proteins Associated with Calcite Deposition in the Bivalve Mytilus Californianus. *Biochemistry* **1983**, *22*, 4139−4145.
(83) Kleineidam, C.; Roces, F. Carbon Dioxide Concentrations and Nest Ventilation in Nests of the Leaf-Cutting Ant Atta Vollenweideri. *Insectes Soc.* **2000**, *47*, 241−248.

https://doi.org/10.1021/acs.cgd.3c00102
Cryst. Growth Des. 2023, 23, 4872−4882